Biosensors and Bioelectronics 40 (2013) 258–264

Contents lists available at SciVerse ScienceDirect

Biosensors and Bioelectronics

journal homepage: www.elsevier.com/locate/bios

Nanowires array modified electrode for enhanced electrochemical detection of nucleic acid

T.S. Ramulu [a], R. Venu [a], B. Sinha [a], B. Lim [a], S.J. Jeon [b], S.S. Yoon [b], C.G. Kim [a,*]

[a] Department of Materials Science and Engineering, Chungnam National University, Daejeon 305-764, South Korea
[b] Department of Physics, Andong National University, Andong 760-749, South Korea

ARTICLE INFO

Available online 28 July 2012

Keywords:
Detection limit
DNA biosensor
Electrodeposition
Nanowire array electrode
Selectivity
Surface area

ABSTRACT

The gold nanowires array electrode (AuNWsA) was synthesized by two step electrodeposition, which provided well oriented vertically aligned nanowires. The dimensions of the nanowires were determined by scanning electron micrograph and found to be around 1.5 μm in length with 200 nm diameter. Each nanowire was separated by a distance of 2–3 times the diameter of the nanowire itself. The electrochemical performance of the AuNWsA electrode was evaluated using cyclic voltammetry (CV) and electrochemical impedance spectroscopy (EIS). Using these analytical tools, this AuNWsA electrode was shown to have a high effective surface area and excellent electron transfer surfaces compared with flat bare Au electrode. The AuNWsA electrode was then used as an electrochemical biosensor electrode by immobilizing probe DNA and analyzed by CV, EIS and Fourier transform infrared measurements. The results of this analysis suggested that the AuNWsA electrode provides good surfaces for the immobilization and hybridization of DNA. The selectivity of the probe DNA immobilized AuNWsA electrode was tested using non-complementary and one base pair mismatching DNA. The detection limit of the AuNWsA electrode was determined to be 6.78×10^{-9} M, which is two times smaller than the bare Au electrode.

1. Introduction

Recently, there has been increased interest towards the development of DNA hybridization biosensors which can use to detect nucleic acid sequences for gene analysis, early diagnosis of diseases, biomedical applications and environmental monitoring (Ariksoysa et al., 2005; Carrascosa et al., 2009; Cuccioloni et al., 2008; Tang et al., 2009). Many methods including those based on fluorescence, surface plasma resonance, quartz crystal microbalance, electrochemiluminescence and electrochemical reactions have been used for this purpose (Su et al., 2005; Berdat et al., 2006; Yao et al., 2009; Zhang et al., 2008a; Singh et al., 2011). Among these, the electrochemical methods have been considered as most important since these are known to be simple, sensitive and cost-effective.

The majority of DNA hybridization biosensors has been found to be critically dependent on the availability of the immobilized probe DNA that is accessible on the electrode surface for interaction with the target DNA (Moses et al., 2004; Nakamura et al., 2003). Increasing the amount of probe DNA which is immobilized on the surface in the appropriate molecular orientation would clearly enhance the sensitivity of DNA biosensors (Liu et al., 2005; Taton et al., 2000). Keeping this in view, many efforts have been made to prepare biocompatible nanomaterials for the development of DNA hybridization sensors (Yang et al., 2012; Zhang et al., 2006). In this context, gold nanoparticles, carbon nanotubes and metallic oxides, have been used for signal amplification to improve the selectivity and sensitivity of a DNA biosensor (Zhang et al., 2008b; Hu et al., 2008; Cai et al., 2003; Das et al., 2010). For example, Wang et al. (2011) have developed a biosensor based on a gold nanoflower modified Au electrode and by using this design; the detection limit of the device was achieved with the pM range. Du et al., 2009 constructed a DNA biosensor by immobilizing Au and CdS nanoparticles for signal amplification on Au electrode surfaces and were also able to obtain a detection limit in the pM range. Niu et al., 2008 has used carbon nanotubes modified electrodes for the fabrication of DNA biosensor and reached a detection limit 38.1 pM target DNA. Although several studies have reported for enhancing the sensitivity of DNA biosensors by using nanomaterials, electrode modification with nanomaterials and their performance is still complex. The DNA detection is sometimes difficult in nanomaterials prepared using surfactants and polymers due to the inherent interference. Hence, there is a great need for the development of simple and cost-effective modified electrodes for the detection of DNA with high sensitivity.

Gold nanomaterials are used extensively in biosensors due to their biocompatibility as well as high effective surface area

* Corresponding author. Tel.: +82 42 821 6632; fax: +82 42 822 6272.
E-mail address: cgkim@cnu.ac.kr (C.G. Kim).

0956-5663/$ - see front matter © 2012 Elsevier B.V. All rights reserved.
http://dx.doi.org/10.1016/j.bios.2012.07.034

(Li et al., 2011; Liu et al., 2010). Ordered arrays of gold nanostructure materials have exceptional potential to increase the sensitivity of biosensors (Claussen et al., 2011; Zhang et al., 2009; Yang et al., 2007). One of the most important aspects of fabricating a nanowires array is choosing the fabrication techniques. The ability to control the parameters, like length, diameter, crystallinity and ordered orientation, is highly dependent on the synthesis techniques. Electrochemical deposition is a suitable technique for the synthesis of well aligned nanowires array. Shin et al. (2007) synthesized an array of gold nanopillar electrodes by electrochemical deposition in the nanopore of an anodic aluminum oxide membrane placed on the gold thin film. Hendren et al. (2008) grew arrays of gold nanotubes on a poly pyrrole core on glass substrates. This method requires a secondary template for alignment of the nanotubes. The gold nanowires can be fabricated using an anodic aluminum oxide template by electrochemical deposition for glucose detection (Cheverko and Chung, 2009). However, when this method is used, the surface tension during removal of the template results in the formation of stacks that disturbs the vertical alignment of the nanowires. Sometimes the deposited nanowires are washed out during the template removal process due to poor contact between the sputtered Au film and nanowires. Nanowires array with well vertically aligned and well inter nanowire distances have good electron transfer kinetics. Therefore, a new design of vertically aligned nanowires is desirable for the fabrication of high sensitive biosensors.

In this study, we have developed a DNA biosensor based on vertically aligned gold nanowires array (AuNWsA), which was fabricated by two steps electrodeposition (ED) method. The electrochemical performances of the AuNWsA electrode and the AuNWsA based DNA electrode were investigated by cyclic voltammetry (CV) and electrochemical Impedance spectroscopy (EIS). The detection limit of the DNA biosensor fabricated by AuNWsA was tested by differential pulse voltammetry (DPV).

2. Experimental details

2.1. Materials and chemicals

Nucleopore track-etched polycarbonate (PC) membranes with 200 nm in diameter was procured from Whatman. The gold plating solution was purchased from SME, Korea. Potassium ferricyanide [$K_3Fe(CN)_6$], potassium ferrocyanide [$K_4Fe(CN)_6$], and Tris-EDTA buffer (pH 8) was obtained from Sigma Aldrich. All other chemicals were of analytical grade and used without further purification. A 0.05 M phosphate buffer saline (PBS) solution was prepared using Na_2HPO_4 (0.1 M) and NaH_2PO_4 (0.1 M) with 0.15 M of NaCl and adjusted to pH 7.4. A 0.2% chitosan solution was prepared by dissolving 20 mg of chitosan flakes in 10 ml of 0.05 M acetic acid solution at pH 4.5. Deionized water obtained from a Milli-Q water purification system was used throughout the experiments.

All of the oligonucleotides were purchased from GeneChem Inc, Korea. The base sequences used in the present studies are as follows:

1. Thiolated probe DNA (t-DNA): 5′-SH-(CH2)3-TCCGGAGCTGCCC-TACGAGGTCAA-3′
2. Complementary target DNA (c-DNA): 5′-TTGACCTCGTAGGG-CAGCTCCGGA-3′
3. Non-complementary target DNA (nc-DNA): 5′-TGAACGCCGGC-CACGAAGACC-3′
4. One base mismatching target DNA (m-DNA): 5′-TTGACCTCG-TGGGGCAGCTCCGGA-3′

2.2. Apparatus

Electrochemical measurements were performed using an Auto-Lab (EchoChemie, Netherlands) potentiostat/galvanostat. The electrochemical cell consisted of a three electrode system with a AuNWsA electrode as working electrode, a Ag/AgCl reference electrode and a platinum sheet counter electrode. The synthesis of AuNWsA was carried out using an ED system (SP–150, BioLogic, France). The surface morphology and microstructure of AuNWsA were observed by Field emission scanning electron microscope (FE-SEM, Magellan400, FEI company) with an operating voltage of 2 kV. Fourier transform infrared (FTIR) spectra were recorded using an attenuated total reflectance instrument (Brucher Optic GmbH, Germany) for the DNA immobilization and hybridization studies on AuNWsA electrode.

2.3. Fabrication of AuNWsA electrodes

The AuNWsA were fabricated by a two step ED technique using a PC membrane with a pore diameter of 200 nm. The schematic representation of the two step electrochemical synthesis of AuNWsA was shown in Fig. 1(a). Initially, one side of the PC membrane was sputtered with metallic Au for electric conduction, which served as the working electrode. The Au sputtered side of the PC membrane was examined by FE-SEM and showed that the pores of the membrane are not completely covered by sputtered Au, even we sputtered for several tens of minute, which may be due to the high pore diameter of 200 nm (Supporting information, Fig. S1a). Hence, we obtain tubular structures instead of wire structures by conventional electrodeposition (Anandakumar et al. 2011). These results have motivated us to design a new electrochemical deposition procedure.

We employed a two step ED method for fabrication of nanowires. The deposition of the AuNWsA was started with a novel interface-configuration of the "ED solution|| Sputtered Au| PC membrane" by facing the Au sputtered side of the PC membrane up (face up deposition) as shown in the 2nd step in Fig. 1(a). During this face up deposition, the ED was taking place bilaterally, that is, both through the pores forming tubular structures and on the exterior of the PC membrane. During the deposition process the exterior of the PC membrane became thicker with Au film, which completely covered the pores of the PC membrane (Supporting information, Fig. S1b). After 5 h face up, it makes the structure like Au nanotubes on Au film as shown in the 3rd step in Fig. 1 (a). The nanowires deposited into the membrane are made by filling these nanotubes for 10 h through the successive ED under the configuration of "ED solution || PC membrane | Sputtered Au" by facing the Au sputtered side of the PC membrane down (face down deposition) as shown in the 4th–5th steps in Fig. 1(a). The whole ED was performed at potentiostatic mode where the potential of working electrode is held at -1.0 V with respect to the Ag/AgCl reference electrode.

A piece of (0.5 cm^2) AuNWsA embedded in a PC membrane is then attached to the gold coated glass substrate, as shown in Fig. 1(b), by using 0.2% chitosan solution (Yang et al., 2011). To avoid wrinkling and the formation of air bubbles between the nanowire array film and substrate, the attachment step was performed carefully. After drying for about over night, the PC membrane is kept in dichloromethane for several minutes followed by washing with distilled water and allowing for air dry in order to obtain the resultant electrodes (AuNWsA electrode).

2.4. DNA immobilization and hybridization

We employed both chemical and electrochemical pre-treatment for cleaning the bare Au and AuNWsA electrodes (Carvarhal et al.,

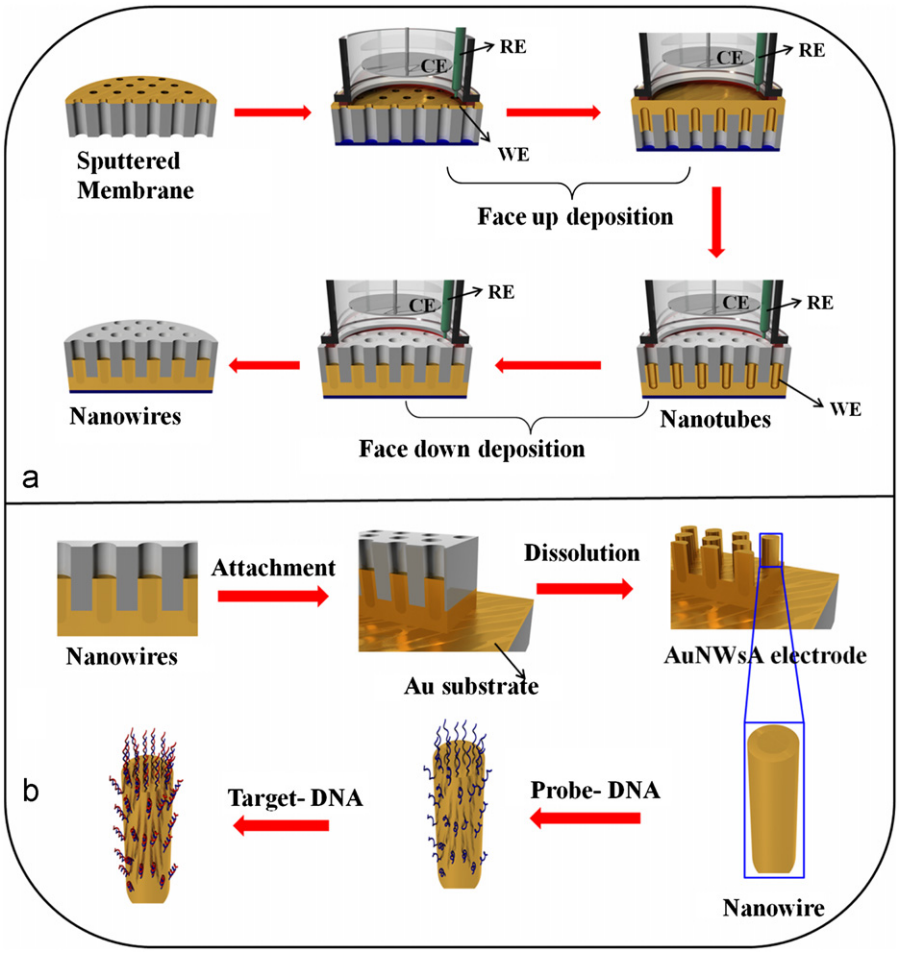

Fig. 1. Schematic illustration of (a) Synthesis of AuNWsA and (b) fabrication of the DNA biosensor electrodes. (WE-working electrode, RE-reference electrode, CE-counter electrode).

2005). The cleaned AuNWsA electrodes are then used to fabricate the DNA biosensor Fig. 1(b). Immobilization of probe DNA on both bare Au and AuNWsA electrode was followed by dispensing 10 μL of 1.3×10^{-5} M probe DNA solution in Tris-EDTA buffer on the surface of the electrodes for 12 h. The electrode was washed with Tris-EDTA buffer to remove any unbound probe DNA. Hybridization to the probe DNA immobilized electrode was accomplished by incubating it with different concentrations of target DNA for 1 h at 37 °C. The bioelectrodes were washed again with Tris-EDTA buffer and stored at 4 °C when it is not in use.

2.5. Electrochemical measurements

All the CV and EIS measurements were performed in a 5 mM $K_3Fe(CN)_6/K_4Fe(CN)_6$ mixture in 0.05 M PBS solution (pH 7.4). The CV measurements were carried out by varying the scan rate from 10 to 100 mVs^{-1} in a potential range 0.6 to −0.4 V. The oxidation signal of the methylene blue accumulation was measured for bioelectrodes using DPV by scanning the potential range of −0.4 to+0.1 in 0.05 M of PBS solution. The impedance spectra of real and imaginary parts of impedance, $Z'(f)$ and $Z''(f)$, were obtained by EIS measurements sweeping the frequency (f) of AC voltage with 10 mV amplitude in the range from 0.1 mHz to 10 kHz under the fixed DC voltage of 0.23 V. All the electrochemical studies were performed at room temperature.

3. Results and discussion

3.1. Fabrication and characterization of AuNWsA

The top and cross sectional FE-SEM images of the free standing AuNWsA electrode are shown in Fig. 2(a and b). The average length of the nanowires is around 1.5 μm. The measured diameter (200 nm) of the nanowires is consistent with the pore size of the PC membrane which was used for the deposition. It can be seen (Fig. 2) that the nanowires are well oriented and highly ordered and vertically aligned to the surface of the thick Au film. The nanowires grown from the Au thick film have been found to be very strong and do not get affected during the chemical etching of PC membrane to obtain vertical alignment of the nanowires array. The spacing between the adjacent nanowires is 2–3 times larger than the diameter of the nanowire itself. It appears that each nanowire perhaps acts as an individual nanoelectrode, which is advantageous for electrochemical measurements of an array type of nanowires (Lin et al., 2004). These free standing Au nanowires have several advantages for electrochemical biosensors compared with flat Au film, because the high effective surface area of these electrodes can be used for immobilization of larger amounts of biomolecules.

3.2. Electrochemical performance of AuNWsA electrode

The electron transfer process of ferricyanide through bare Au and AuNWsA electrodes has been investigated by CV and EIS

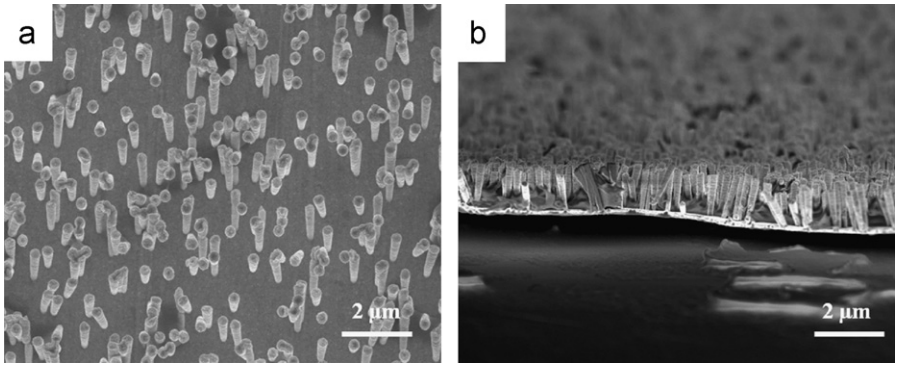

Fig. 2. FE-SEM images of the AuNWsA (a) top view and (b) cross-sectional view.

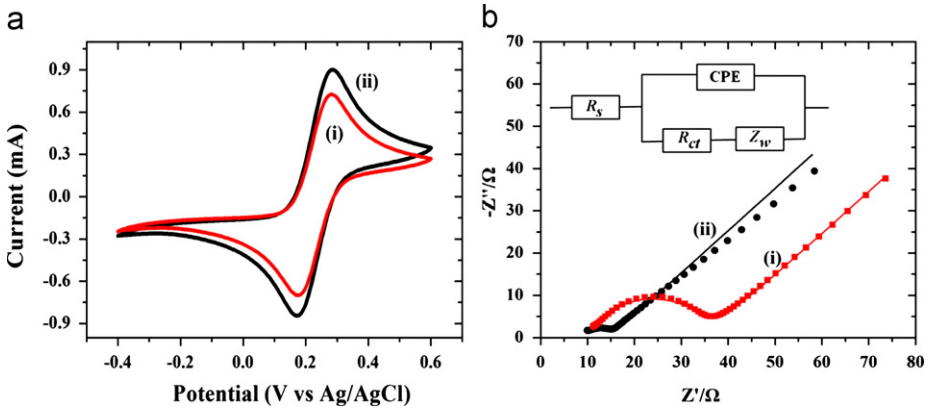

Fig. 3. Cyclic voltagrams (a) and the Nquist plots (b) of bare Au (i) and AuNWsA electrode (ii) in 0.05 M PBS (pH 7.4, 0.15 M NaCl) containing 5 mM $[Fe(CN)_6]^{3-/4-}$.

experiments in 0.05 M PBS solution containing a mixture of 5 mM $K_3Fe(CN)_6/K_4Fe(CN)_6$. The cyclic voltagrams of both bare Au and AuNWsA electrode at a scan rate of 20 mVs^{-1} is shown in Fig. 3a. The bare Au electrode exhibited a pair of well-defined redox peaks with an anodic (E_{pa}) and cathodic (E_{pc}) peak potential of 0.28 V and 0.17 V, respectively. In addition, the anodic peak current (I_a) is found to be 0.726 mA. These peaks are attributed to the redox behavior of $[Fe(CN)_6]^{3-/4-}$ at electrode surfaces.

In a similar way, the AuNWsA electrode also contained a well-defined anodic peak and cathodic peak with 0.9 mA of I_a. The increase in I_a of the AuNWsA electrode with respect to the bare Au electrode may be due to the large surface area of the three-dimensional array type wires, which can increase the active surface area (Wang et al., 2009). Besides this, surface roughness of the AuNWsA electrode may be another factor to the enhanced electron transfer process for redox probe (Creager et al., 1992). It appears that at the bare Au electrode surface, linear diffusion occurs and the ions are perhaps trapped on the surface during electrochemical reaction. However, at the AuNWsA electrode surface, 3 dimensional radial diffusion occurs leading to enhanced binding of ions (Lin et al., 2008). The vertically aligned nanowires on electrode surfaces can function as an "electron antennae" and enhance the electron transfer rate by promoting the electron transfer between $[Fe(CN)_6]^{3-/4-}$ and the electrode (Zhao et al., 2008).

The EIS could provide the information on the impedance changes of both electrode surfaces. The Nyquist plots [$Z'(f)$ vs $-Z''(f)$] from the EIS are shown in Fig. 3b. The Nyquist plots display the typical curves; a straight line at the low frequency region indicating diffusion controlled process and a semicircle at the high frequency region indicating a charge transfer process. This spectrum can be represented by the Randles equivalent circuit (inset in Fig. 3b), where R_s is the resistance of the bulk electrolyte and R_{ct}, Z_w and CPE are the charge transfer resistance, Warburg impedance and constant phase element, respectively (Shervedani and Mozaffari, 2006). Considering the influence of surface roughness, CPE element is used to describe the double layer capacitance, instead of pure capacitance.

The admittance of CPE element is represented by $Y=Y_o(j\omega)^n$, where $\omega=2\pi f$ is angular frequency and $j=(-1)^{1/2}$. The straight lines in Fig. 3b are the simulated curve obtained by complex nonlinear curve fitting the measured impedance spectra with the equivalent circuit. The simulated curves show good agreement with experimental EIS spectra. The R_{ct}, obtained from the curve fitting, for the bare Au electrode was about 25.578 Ω (Fig. 3b, curve i) and the R_{ct} value for AuNWsA electrode was decreased to 5.91 Ω (Fig. 3b, curve ii). The decrease in R_{ct} for AuNWsA electrode may be due to the surface roughness, radial diffusion of ions or synergitic effect (Liu et al., 2009). The other EIS parameters of the equivalent circuit obtained by the curve fitting are given in the supplementary information (Table 1).

3.3. DNA immobilization and hybridization

The cyclic voltagrams obtained at a scan rate of 20 mVs^{-1} for AuNWsA electrode (i), thiolated probe DNA immobilized on AuNWsA electrode (ii, AuNWsA/t-DNA) and hybridized complimentary DNA (iii, AuNWsA/t-DNA/c-DNA) electrodes are shown in Fig. 4a. The AuNWsA electrode produces a well defined cathodic peak and anodic peak at in the potential range of 0.6 to −0.4 V with a I_a of 0.9 mA (curve i). However, the immobilization of thiolated probe DNA on the AuNWsA electrode surface results in a decrease in the peak current (0.622 mA), indicating that the probe DNA was successfully immobilized on

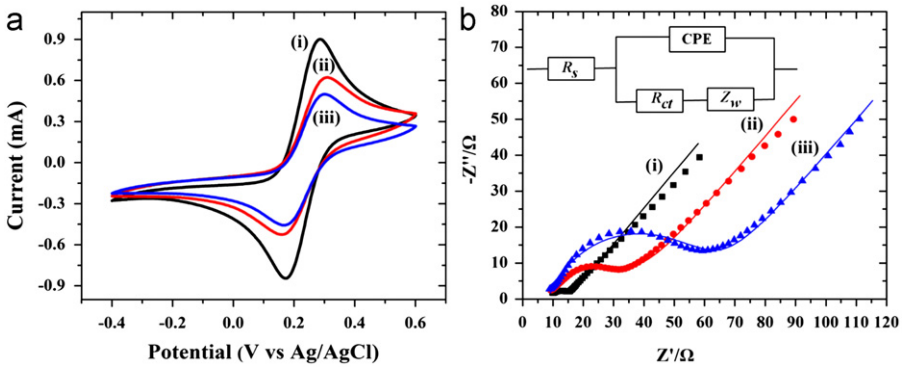

Fig. 4. Cyclic voltagrams (a) and the Nquist plots (b) of AuNWsA (i), AuNWsA/t-DNA (ii) AuNWsA/t-DNA/c-DNA (iii) electrodes in 0.05 m PBS (pH 7.4, 0.15 M NaCl) containing 5 mM $[Fe(CN)_6]^{3-/4-}$.

the AuNWsA electrode surfaces (curve ii). The decrease in the peak current of AuNWsA/t-DNA is perhaps due to repulsion between the $[Fe(CN)_6]^{3-/4-}$ species and the negatively charged phosphate back bone of the AuNWsA/t-DNA. A further decrease in the peak current (0.502 mA) was observed when the complementary DNA was hybridized with the probe DNA (curve iii). This perhaps occurs due to the introduction of the complementary DNA which in turn increases the negative charge of the phosphate skeleton, indicating increased repulsion of the redox species on electrode surface (Wang et al., 2011).

The Nyquist plots from the EIS measurements and the simulated fitting curves of AuNWsA (i) AuNWsA/t-DNA (ii) and AuNWsA/t-DNA/c-DNA (iii) electrodes are shown in Fig. 4b. The R_{ct} value of AuNWsA electrode was very small (5.91 Ω) (curve i) and the R_{ct} value of the probe DNA immobilized electrode is relatively high (30.587 Ω), which may have occurs because the electro-negative phosphate skeleton of the DNA prevented the electron transfer process of $[Fe(CN)_6]^{3-/4-}$ at the electrode surface during the redox chemical reaction (curve ii). A further increase in the R_{ct} (54.428 Ω) value for AuNWsA/t-DNA/c-DNA is observed. This likely occurs because the hybridization of complimentary DNA with probe DNA increased the electro-negative phosphate skeleton, which is the responsible for repulsive force between $[Fe(CN)_6]^{3-/4-}$ at electrode surfaces. The comparison of EIS parameters is given in the supplementary information (Table 1).

3.4. Immobilization and hybridization confirmation through FT-IR analysis

The FT-IR spectroscopic studies were performed for further confirmation of immobilization and hybridization of nucleic acid on the AuNWsA electrode surfaces. The FT-IR spectra of AuNWsA/t-DNA and AuNWsA/t-DNA/c-DNA bioelectrodes are shown in Fig. 5(a and b). In previous FT-IR spectroscopic studies, characteristic peaks of DNA were observed in the range of 900–1800 cm^{-1} (Wang et al., 2001). The FT-IR spectra of AuNWsA/t-DNA bioelectrode exhibits absorption peaks at 1729, 1459 and 1277 cm^{-1}, which corresponded to the functional groups of DNA, such as the carboxylic group in thymine and guanine, in-plane imidazole ring vibration in adenine, cytosine and guanine, and pyrimidine ring vibration in thymine and cytosine, respectively.

The absorption peak at 1596 cm^{-1}, which corresponds to the in-plane ring vibration modes of C–C and C=N in adenine and cytosine, was diminished on the AuNWsA/t-DNA bioelectrode. This may be due to the presence of lower amounts of t-DNA on the AuNWsA. Apart from this, the absorption peaks corresponding to complementary DNA hybridized on the AuNWsA/t-DNA bioelectrode shows similar absorption peaks with increased peak intensities than the AuNWsA/t-DNA bioelectrode. The absorption peaks

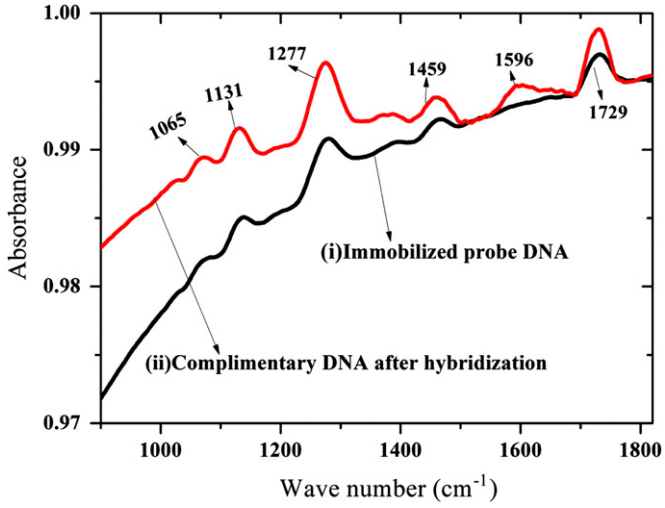

Fig. 5. FT-IR spectra of (a) AuNWsA/t-DNA electrode (b) and AuNWsA/t-DNA/c-DNA electrode.

observed at 1065 and 1131 cm^{-1} correspond to stretching vibrations of PO_4^- groups of the phosphodiester deoxyribose backbone (Patel et al., 2009). These results indicate that the DNA probe is successfully immobilized on the AuNWsA electrode surfaces.

3.5. Selectivity and detection of various target DNA concentrations

The DPV measurements were conducted for the thiolated probe DNA immobilized on AuNWsA (i, AuNWsA/t-DNA), hybridized complimentary DNA (ii, AuNWsA/t-DNA/c-DNA), non-complementary DNA (iii, AuNWsA/t-DNA/nc-DNA) and one base pair mismatching (iv, AuNWsA/t-DNA/m-DNA) electrode surfaces in 0.05 M PBS (pH 7.4) containing 20 μM methylene blue (MB) as a redox indicator (Fig. 6a). The bioelectrodes are kept for 5 min in methylene blue solution prior to the DPV measurements. A considerable decrease in the magnitude of the MB peak current (I_p) is observed for AuNWsA/t-DNA/c-DNA (curve ii) compared to the AuNWsA/t-DNA (curve i), indicating a lower MB accumulation on the electrode surface during the hybridization process. The decrease in I_p for the duplex complex may be due to the steric hindrance and conformational changes of double strand DNA, that may inhibit MB accumulation (Singh et al., 2010). The higher I_p observed for the AuNWsA/t-DNA electrode may be due to the strong affinity of the MB to the outside guanine bases of t-DNA.

The selectivity of the AuNWsA/t-DNA bioelectrode was examined in a controlled experiment where the I_p values were changed by incubating with nc-DNA and m-DNA. The I_p value of the

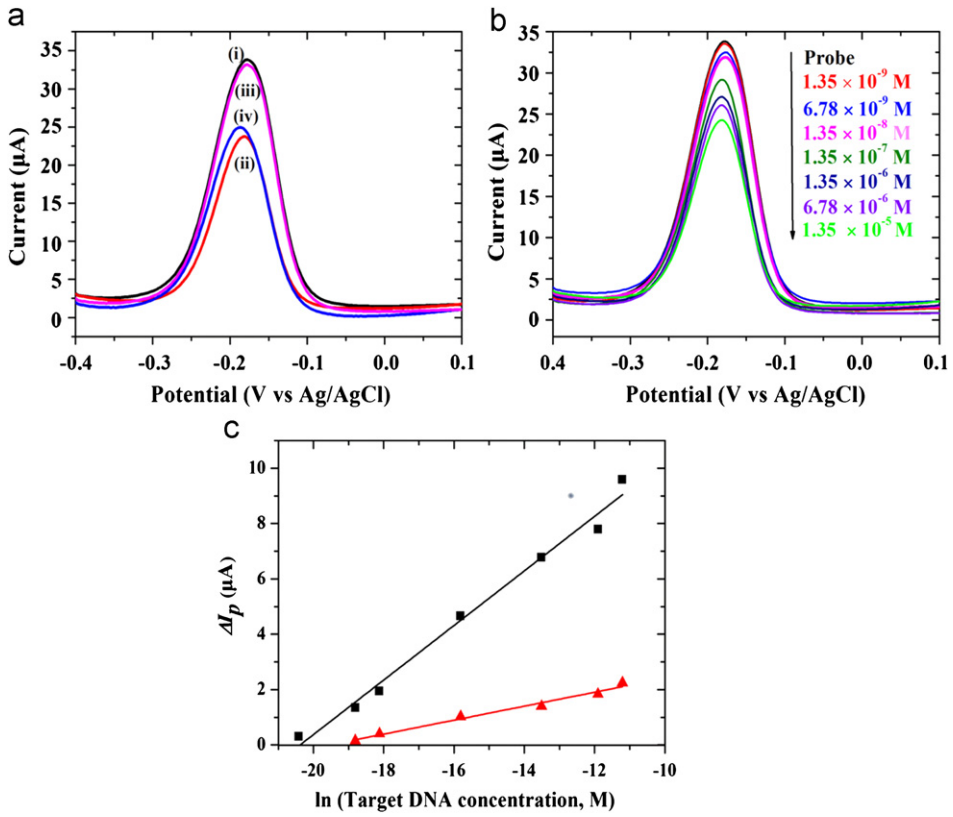

Fig. 6. (a) Differential pulse voltagrams of (i) AuNWsA/t-DNA (ii) AuNWsA/t-DNA/c-DNA (iii) AuNWsA/t-DNA/nc-DNA(iv) AuNWsA/t-DNA/m-DNA electrodes; (b) DPV measurements of AuNWsA/t-DNA electrode after hybridization with different concentrations of complimentary sequence in 0.05 M PBS (pH 7.4, 0.15 M NaCl) containing 20 μM methylene blue and (c) ΔI_p as a function of *ln*(target DNA concentration) of (i) bare Au electrode (ii) and AuNWsA electrode.

AuNWsA/t-DNA/nc-DNA electrode does not change significantly, indicating the absence of a duplex complex on the electrode surface (curve iii). The small increase in I_p for the AuNWsA/t-DNA/m-DNA electrode compared to the AuNWsA/t-DNA/c-DNA electrode may be due to the placing of mismatching in the DNA sequence (curve iv), since the stability of the DNA duplex depends on the location of the mismatch, its nearest neighbor and its orientation (Singh et al., 2011). The difference in current density for AuNWsA/t-DNA/c-DNA and AuNWsA/t-DNA/nc-DNA has been found to be 18 $\mu A cm^{-2}$ (surface area = 0.5 cm^2). The change in signal from c-DNA to m-DNA is found to be 11%, which is a significant change (Ahangar and Mehrgardi, 2011).

The DPV measurements conducted as a function of target DNA concentration (c) ranging from 1.356×10^{-9} M to 1.356×10^{-5} M for AuNWsA/t-DNA bioelectrode are shown in Fig. 6b. The height of the MB peak increases with a decrease in the target DNA concentration, This may be due to the lower hindrance of the MB-guanine interaction in the hybridization process of low concentration complementary DNA. The MB peak height at target DNA concentrations $\leq 1.356 \times 10^{-9}$ M has been observed to be same as the peak height of the probe DNA, which reveals the absence of the target DNA on the electrode surface.

A linear correlation of the differences in peak currents, $\Delta I_p(c) = I_p(c=0) - I_p(c)$, with respect to the natural logarithm of target DNA concentration for both AuNWsA electrode and bare Au electrode are shown in Fig. 6(c). It can be seen that AuNWsA/t-DNA bioelectrode is more sensitive and exhibits a lower detection limit than the bare Au electrode sensor. The detection limit, at which $\Delta I_p(c)$ approaches zero, was determined to be 6.78×10^{-9} M for the AuNWsA/t-DNA bioelectrode and 1.356×10^{-8} M for the bare Au bioelectrode. This indicates that the detection limit of the AuNWsA was two times smaller than the bare Au electrode. The DPV measurements observed as a function of target DNA concentrations ranging from 6.78×10^{-9} M to 1.356×10^{-5} M probe immobilized bare Au electrode is shown in the supporting information (Fig. S2). The reproducibility of probe DNA immobilized on both bare Au and AuNWsA electrode for the detection of hybridized target DNA are measured by DPV. Depending on the I_p values, the average and standard deviation of ΔI_p for AuNWsA electrode are 1.329–9.395 μA and 0.009–0.172 μA, respectively (Table 2, supplementary information). The stability and reproducibility of AuNWsA/t-DNA bioelectrode is given in supplementary information (Fig. S3).

4. Conclusion

The AuNWsA electrode has been fabricated by a two step ED method using a novel electrolyte and PC membrane interface. The length and diameter of the nanowires are found to be 1.5 μm and 200 nm, respectively. The morphological studies of AuNWsA reveal that the nanowires are well-aligned and strongly attached to the Au thick film. The developed electrochemical DNA biosensor provides an excellent response for the detection of specific hybridized DNA in a low concentration (6.78×10^{-9} M), which is two times lower than the detection limit of the Au electrode. The fabricated DNA biosensor exhibits good selectivity and stability. This AuNWsA electrode can be used for the development of enzyme and protein biosensors.

Acknowledgment

This research was supported by WCU (World Class University) program through the National Research Foundation of Korea

funded by the Ministry of Education, Science and Technology (R32-20026).

Appendix A. Supporting information

Supplementary data associated with this article can be found in the online version at http://dx.doi.org/10.1016/j.bios.2012.07.034.

References

Ahangar, L.E., Mehrgardi, M.A., 2011. Electrochimica Acta 56, 10264–10269.
Anandakumar, S., Sudharani, V., Ramulu, T.S., Yang, H.J., Lim, B.H., Kim, J., Yoon, S.S., Kim, C.G., 2011. Journal of The Electrochemical Society 158, E124–E127.
Ariksoysa, D.O., Karadeniz, H., Erdem, A., Sengonul, A., Sayiner, A.A., Ozsoz, M., 2005. Analytical Chemistry 77, 4907–4917.
Berdat, D., Marin, A., Herrera, F., Gijs, M.A.M., 2006. Sensors and Actuators B 118, 53–59.
Cai, H., Cao, X., Jiang, Y., Fang, P.H.Y., 2003. Analytical and Bioanalytical Chemistry 375, 287–293.
Carrascosa, L.G., Calle, A., Lechuga, L.M., 2009. Analytical and Bioanalytical Chemistry 39, 1173–1182.
Carvarhal, R.F., Freire, R.S., Kubato, L.T., 2005. Electroanalysis 17, 1251–1259.
Cheverko, S., Chung, C.H., 2009. Sensors and Actuators B 142, 216–223.
Claussen, J.C., Wickner, M.M., Fisher, T.S., Porterfield, D.M., 2011. ACS Applied Materials and Interfaces 3, 1765–1770.
Creager, S.E., Hockett, L.A., Rowe, G.K., 1992. Languimer 8, 854–861.
Cuccioloni, M., Mozzicafreddo, M., Barocci, S., Ciuti, F., Pecorelli, I., Eleuteri, A.M., Spina, M., Fioretti, E., Angeletti, M., 2008. Analytical Chemistry 80, 9250–9256.
Das, M., Sumana, G., Nagarajan, R., Malhotra, B.D., 2010. Applied Physics Letters 96 133703-1-3.
Du, P., Li, H., Mei, Z., Liu, S., 2009. Bioelectrochemistry (Amsterdam, Netherlands) 75, 37–43.
Hendren, W.R., Murphy1, A., Evans, P., Connor, D.O., Wurtz, G.A., Zayats, A.V., Atkinson, R., Pollard, J., 2008. Journal of Physics Condensed Matter: an Institute of Physics Journal 20, 362203–362207.
Hu, K., Lan, D., Li, X., Zhang, S., 2008. Analytical Chemistry 80, 9124–9130.
Li, F., Han, X., Liu, S., 2011. Biosensors and Bioelectronics 26, 2619–2625.
Lin, C.C., Juo, T.J., Chen, Y.J., Chiou, C.H., Wang, H.W., Liu, Y.L., 2008. Desalination 233, 113–119.
Lin, Y., Lu, F., Tu, Y., Ren, Z., 2004. Nano Letters 4, 191–195.
Liu, S., Liu, J., Han, X., Cui, Y., Wang, W., 2010. Biosensors and Bioelectronics 25, 1640–1645.
Liu, S.F., Li, Y.F., Li, J.R., Jiang, L., 2005. Biosensors and Bioelectronics 21, 789–795.
Liu, Y., Zhu, Y., Zheng, Y., Xu., Fangfang., 2009. Nanoscale Research Letters 4, 21–215.
Moses, S., Brewer, S.H., Lowe, L.B., Lappi, S.E., Gilvey, L.B.G., Sauthier, M., Tenent, R.C., Feldheim, D.L., Franzen, S., 2004. Languimer 20, 11134–11140.
Nakamura, F., Ito, E., Sakao, Y., Ueno, N., Gatuna, I.N., Ohuchi, F.S., Hara, M., 2003. Nano Letters 3, 1083–1086.
Niu, S., Zhao, M., Hu, L., Zhang, S., 2008. Sensors and Actuators B 135, 200–2005.
Patel, M.K., Solanki, P.R., Seth, S., Gupta, S., Khare, S., Kumar, A., Malhotra, B.D., 2009. Electrochemistry Communications 11, 969–973.
Shervedani, R.K., Mozaffari, S.A., 2006. Analytica Chimica Acta 2006, 223–228.
Shin, C., Shin, W., Hong, H.G., 2007. Electrochimica Acta 53, 720–728.
Singh, R., Sumanna, G., Verma, R., Sood, S., Pandey, M.K., Gupta, R.K., Malhotra, B.D., 2010. Journal of Biotechnology 150, 357–365.
Singh, R., Verma, R., Kaushik, A., Sumana, G., Sood, S., Gupta, R.K., Malhotra, B.D., 2011. Biosensors and Bioelectronics 26, 2967–2974.
Su, X., Wu, Y.J., Robelek, R., Knoll, W., 2005. Langmuir: the ACS Journal of Surfaces and Colloids 21, 348–353.
Tang, L., Zeng, G., Shen, G., Li, Y., Liu, C., Li, Z., Luo, J., Fan, C., Yang, C., 2009. Biosensors and Bioelectronics 24, 1474–448-79.
Taton, T.A., Mirkin, C.A., Letsinger, R.L., 2000. Science (New York, NY) 289, 1757–1760.
Wang, Z., Liu, D., Dong, S., 2001. Biophysical Chemistry 89, 87–94.
Wang, H., Wang, X., Zhang, X., Qin, X., Zhao, Miao, Z., Huang, N., Chen, Q., 2009. Biosensors and Bioelectronics 25, 142–146.
Wang, L., Chen, X., Wang, X., Han, X., Liu, S., Zhao, C., 2011. Biosensors and Bioelectronics 30, 151–157.
Yang, G., Chen, Y., Li, L., Yang, Y., 2011. Clinica Chimica Acta: International Journal of Clinical Chemistry 412, 1544–1549.
Yang, J., Wang, X., Shi, H., 2012. Sensors and Actuators B 162, 178–183.
Yang, M., Qu, F., Li, Y., He, Y., Shen, G., Yu, R., 2007. Biosensors and Bioelectronics 23, 414–420.
Yao, W., Wang, L., Wang, H., Zhang, X., Li, L., 2009. Michrochim Acta 165, 407–413.
Zhang, J., Song, S., Zhang, L., Wang, L., Wu, H., Pan, D., Fan, C., 2006. Journal of the American Chemical Society 128, 8575–8580.
Zhang, J., Lao, R., Song, S., Yan, Z., Fan, C., 2008a. Analytical Chemistry 80, 9029–9033.
Zhang, S., Zhong, H., Ding, C., 2008b. Analytical Chemistry 80, 7206–7212.
Zhang, X., Li, D., Bourgeois, L., Wang, H., Webley, P.A., 2009. ChemPhysChem 10, 436–441.
Zhao, W., Sun, S.X., Xu, J.J., Chen, H.Y., Cao, X.J., Guan, X.H., 2008. Analytical Chemistry 80, 3769–3776.